Supporting Information for

A new ultrafast superionic Li-conductor: Ion dynamics in $Li_{11}Si_2PS_{12}$ and comparison with other tetragonal LGPS-type electrolytes

*Alexander Kuhn,[a] Oliver Gerbig,[a] Changbao Zhu,[a] Frank Falkenberg,[a] Joachim Maier,[a] and Bettina V. Lotsch[a,b,c]**

[a] *Max Planck Institute for Solid State Research, Heisenbergstr. 1, 70569 Stuttgart, Germany.*
[b] *Department of Chemistry, Ludwig-Maximilans-Universität München, Butenandtstr. 5-13, 81377 München, Germany.*
[c] *Nanosystems Initiative Munich and Center for Nanoscience, Schellingstr. 4, 81377 München, Germany*

S1: Experimental

Preparation of $Li_{10}SnP_2S_{12}$:

The starting materials for the synthesis were Li_2S (Alfa Aesar, 99.9 %), P (Alfa Aesar, 98.9 %), S (Alfa Aesar, 99.5%), and Sn (Alfa Aesar, 99.995%). The dry starting materials were first mechanically treated in a ball mill under argon for 2 days. Pellets were pressed from the obtained amorphous precursor and heated in an evacuated quartz ampoule according to the following temperature program: 30 Kh^{-1} → 613 K (10h) → 30 Kh^{-1} → 653 K (10h) → 30 Kh^{-1} → 723 K (2d). In the first step at 613 K, the material crystallizes in the orthorhombic modification (cf. Li_4SnS_4[1]) which then transforms to the desired tetragonal structure at 653 K. The subsequent sintering step at 723 K improves the crystallinity of the sample.

Preparation of $Li_{11}Si_2PS_{12}$:

The preparation of phase-pure hypothetical tetragonal $Li_{10}SiP_2S_{12}$ was not successful by means of a conventional solid-state approach. Instead, the main phase at all temperatures between 573 K and 1023 K was the orthorhombic modification of the LSiPS solid solution (reported by Kanno *et al*. in 2002).[2] The fact that the tetragonal modification has a slightly higher density than the orthorhombic one and the fact that a higher Si content should enhance the stability we assumed that tetragonal $Li_{10}SiP_2S_{12}$ should be accessible via high-pressure synthesis. Indeed, the XRD pattern after high-pressure treatment of orthorhombic $Li_{10}SiP_2S_{12}$ shows the reflections of tetragonal LSiPS besides residual reflections of the orhtorhomic modification. An EDX analysis of the product revealed demixing of Si and P in different crystallites: some crystallites (ascribed to the tetragonal modification) showed the composition $Li_{11}Si_2PS_{12}$ while others were depleted with Si. (Before the high-pressure treatment, the Si and P were homogeneously distributed). Indeed, when orthorhombic $Li_{11}Si_2PS_{12}$ is used as a starting material for the high-pressure treatment, almost phase-pure tetragonal $Li_{11}Si_2PS_{12}$ is obtained.

The starting materials for the synthesis were Li_2S (Alfa Aesar, 99.9 %) Si (Aldrich, 99.9995%), P (Alfa Aesar, 98.9 %), and S (Alfa Aesar, 99.5%). The dry starting materials were first mechanically treated in a

ball mill under argon for 3 days. Pellets were pressed from the obtained amorphous precursor and heated in an evacuated quartz ampoule at 823 K for 4 days. The obtained orthorhombic $Li_{11}Si_2PS_{12}$ was transformed into tetragonal $Li_{11}Si_2PS_{12}$ via high-pressure treatment at 723 K with pressures in the range $3 < p < 5$ GPa.

General Experimental Details / Instruments:

Due to the moisture and air sensitivity of the materials, all preparation and analysis steps were performed under inert Ar atmosphere. The mechanical treatment was performed with a Fritsch Premium Line 5 planetary ball mill with a zirconia vial and zirconia balls in an air-tight steel container. For the high-temperature treatment, pellets were pressed and vacuum-sealed in silica glass tubes. For the high-pressure treatment of the LSiPS sample, the precursor material was tightly filled into and precompacted in a Au crucible (ø 4mm). While it was heated to temperatures from 623 to 823 K for 10h a pressure of up to 5 GPa was applied to the crucible in a Belt- type press. XRD was performed with a STOE Stadi P diffractometer working in Debye-Scherrer geometry with Mo $K_{\alpha 1}$ or Cu $K_{\alpha 1}$ radiation (Ge(111) monochromator). For the Rietveld refinement, DiffracPlus TOPAS v4.2 (Bruker AXS) was used. NMR measurements were performed with a Bruker Avance II spectrometer connected to cryomagnets of 9.4 T. For ^{31}P MAS measurements, commercial Bruker MAS probes with rotors of 4 mm or 2.5 mm diameter were used ($\nu_{rot} = 12$ kHz). The measurements were performed with a one-pulse sequence and a sufficiently long recycle delay to allow complete relaxation. For ^{7}Li PFG NMR, ^{7}Li NMR line shape, and ^{7}Li NMR relaxometry, a Bruker Diff60 probe was used. For the PFG measurements a stimulated echo pulse sequence with two gradient pulses of variable strength separated by the diffusion time Δ was used. The attenuation of the echo was analyzed using the Stejskal-Tanner equation for 3D diffusion[3] as previously described in detail in Ref. [4]. Impedance spectroscopy was performed using a Novocontrol Alpha Analyzer and a home-built impedance cell. For the measurement, a pellet was cold-pressed from the powdered sample by applying a uniaxial pressure and subsequently annealed at 583 K for 1 day. Li-blocking Au electrodes were sputtered on the surfaces of the pellet. Before the measurement, the pellet was annealed at 310°C, again. For the dc polarization measurement, a Keithley 614 Electrometer and a Keithley 220 current source were used.

S2: Rietveld refinement results:

Below, the Rietveld refinement results of $Li_{10}SnP_2S_{12}$ and $Li_{11}Si_2PS_{12}$ are displayed. Only the heavy atoms P, Si/Sn, and S atoms are listed since the light Li atoms were not subject to the refinement. For Li, the values as reported for $Li_{10}GeP_2S_{12}$ from single-crystal diffraction[5] were used and kept constant for the refinement since a refinement of the Li positions is not possible from the powder data.

$Li_{11}Si_2PS_{12}$

radiation: Cu $K_{\alpha 1}$

space group *P4₂/nmc* (137:1)

Tetragonal, $a = b = 8.6905(14)$ Å, $c = 12.5703(20)$ Å

Pos.	Wyck.	*x*	*y*	*z*	*occ.*	B_{eq} (Å^2)
Si1	4*d*	0	0.5	0.68902(68)	1[*]	2.55(24)
{P1	4*d*	0	0.5	= *z*(Si1)	=1-*occ*(Si1)	= B_{eq}(Si1) }
P2	2*b*	0	0	0.5	1	2.23(34)
S1	8*g*	0	0.18792(58)	0.40579(52)	1	2.31(15)
S2	8*g*	0	0.29602(53)	0.09812(47)	1	2.04(15)
S3	8*g*	0	0.69826(66)	0.79178(42)	1	1.10(15)

$R_{exp} = 5.82$ %, $R_{wp} = 7.92$ %, $R_p = 5.99$ %, $R_{Bragg} = 2.926$ %, $GoF = R_{wp} / R_{exp} = 1.36$

[*] since Si^{IV} and P^V are isoelectronic they cannot be distinguished in XRD. According to ^{31}P MAS results, the 4*d* site is partially occupied by P (approx. 5%).

$Li_{10}SnP_2S_{12}$

radiation: Mo $K_{\alpha 1}$

space group *P4₂/nmc* (137:1)

Tetragonal, $a = b = 8.7506(18)$ Å, $c = 12.7993(28)$ Å

Pos.	Wyck.	*x*	*y*	*z*	*occ.*	B_{eq} (Å^2)
Sn1	4*d*	0	0.5	0.68493(26)	0.4694(66)	2.03(12)
P1	4*d*	0	0.5	= *z*(Sn1)	=1-*occ*(Sn1)	= B_{eq}(Sn1)
P2	2*b*	0	0	0.5	1	3.59(44)
S1	8*g*	0	0.185938(54)	0.40698(44)	1	3.72(20)
S2	8*g*	0	0.28552(55)	0.09415(52)	1	3.93(19)
S3	8*g*	0	0.71001(54)	0.79043(37)	1	3.21(20)

$R_{exp} = 3.55$ %, $R_{wp} = 5.87$ %, $R_p = 4.53$ %, $R_{Bragg} = 2.588$ %, $GoF = R_{wp} / R_{exp} = 1.66$

S3 Tables:

Table S1. Experimental cell parameters of tetragonal LGPS-type materials determined at room temperature.

Comound	*a* / Å	*c* / Å	*a* / *c*	*V* / Å^3
$Li_{11}Si_2PS_{12}$[a]	8.695	12.568	1.445	949
$Li_{10}GeP_2S_{12}$[b]	8.710	12.603	1.447	956
Li_7GePS_8[b]	8.719	12.662	1.452	962
$Li_{10}SnP_2S_{12}$[a]	8.751	12.799	1.463	980

[a] this work, [b] Ref. [4]

Table S2: Room-temperature bulk conductivities and activation energies for LGPS-type electrolytes.

Compound	$\sigma_{298\,K}$ / (mS/cm)	E_A / eV
$Li_{11}Si_2PS_{12}$[a]	-	-
$Li_{10}GeP_2S_{12}$[b]	8	0.22
Li_7GePS_8[b]	7	0.22
$Li_{10}SnP_2S_{12}$[a]	4	0.25
$Li_{10}SnP_2S_{12}$[c]	7	0.27

[a] this work, [b] taken from Ref. [4], [c] Ref. [6]

Table S3: Onset temperatures T_{MN} of the motional narrowing of the ^{7}Li NMR central transition, jump rates τ^{-1}at T_{MN}, as well as activation energies estimated from T_{MN} using the Waugh-Fedin expression.[2]

Compound	T_{MN} / K	$\tau^{-1}(T_{MN})$ s^{-1}	E_A / eV
$Li_{11}Si_2PS_{12}$[a]	125	1.5×10^4	-
$Li_{10}GeP_2S_{12}$[b]	135	1.4×10^4	0.22
Li_7GePS_8[b]	135	1.4×10^4	0.22
$Li_{10}SnP_2S_{12}$[a]	145	1.4×10^4	0.25

[a] this work, [b] taken from Ref. [4]

S4: Further details of the NMR relaxometry study:

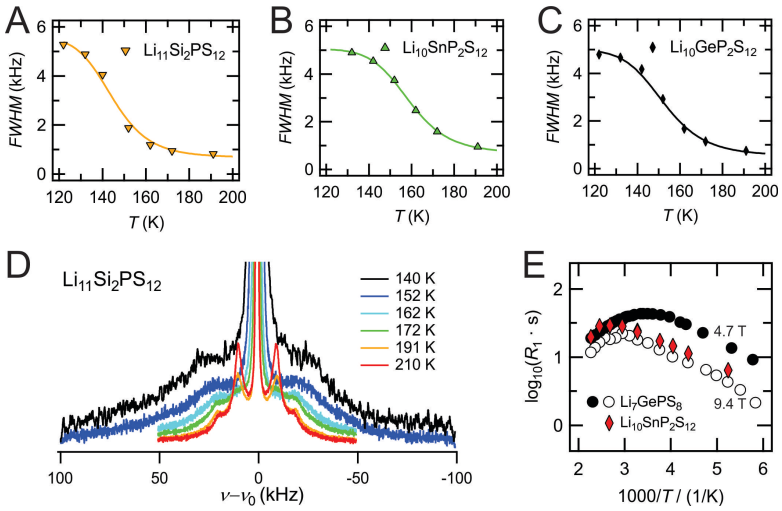

Figure S1: (A-C) temperature dependent full width at half maximum (*fwhm*) of the ^{7}Li NMR central transition for LSiPS, LSnPS, and LGPS[4]. (D) Temperature-dependent ^{7}Li NMR satellite transition for LSiPS. (E) Temperature-dependent longitudinal ^{7}Li NMR relaxation rates R_1 of LSnPS in comparison with LGPS[4].

Fig. S1 (A-C) shows the temperature dependent *fwhm* (full width at half maximum) of the ^{7}Li NMR central transitions. From the onset of narrowing at T_{MN}, an absolute jump rate can be determined from the narrowing condition $\tau^{-1} \approx \sqrt{M_{2\,\text{rigid lattice}}}$[7] and an activation energy can be roughly estimated using the empirical expression by Waugh and Fedin, $E_A \approx 1.61 \cdot 10^3 \cdot T_{MN} \cdot \text{eV/K}$.[8] The values obtained from the narrowing curves in Fig. (A-C) are summarized in Table S3. Fig. S1 (D) shows the temperature-dependent satellite transitions for the LSiPS sample. At low temperatures, a broad foot is observed which represents the quadrupolar coupling of the quadrupolar moment of the ^{7}Li spins with the respective electric field gradients at the different Li sites. At higher temperatures, due to Li ion dynamics, the electric field gradients are averaged. From the onset of the averaging, a jump rate can be deduced as outlined above for the narrowing of the central transition. In Fig. S1 (E), the temperature dependent longitudinal ^{7}Li NMR relaxation rates R_1 of LSnPS measured at an external magnetic field of $B_0 = 9.4$ T are displayed in comparison with those of LGPS.[4] From the rate maximum, a jump rate can be deduced according to the maximum condition $\tau^{-1} \approx \omega_0 = \gamma B_0$.[7] Here, a jump rate of $\tau^{-1} = 9.76 \times 10^8$ s^{-1} at $T_{max} = 360$ K is obtained. As expected, the relaxation rate maximum for LSnPS is observed at slightly higher temperatures than for LGPS[4].

S5: Further details of the impedance spectroscopy study:

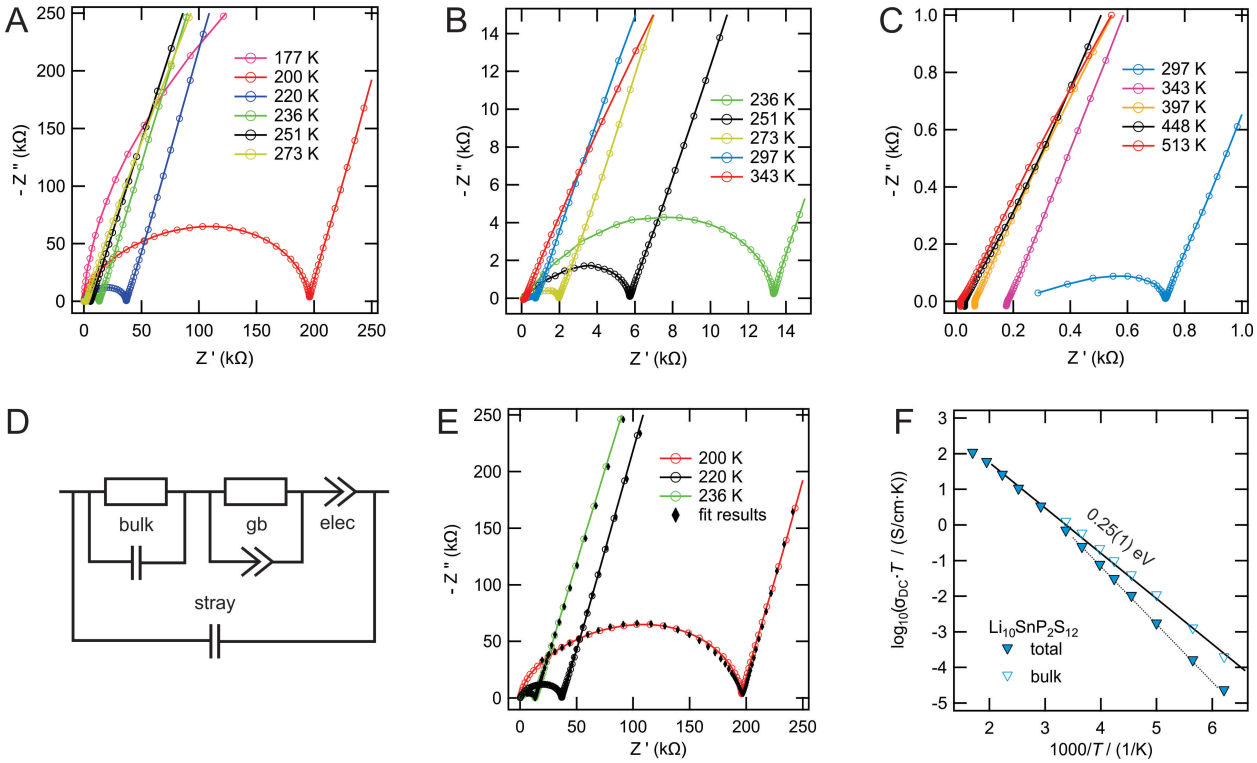

Figure S2: (A-C) Complex impedance plots of temperature-dependent impedance spectroscopy data of LSnPS. (D) Equivalent circuit used to separate bulk, grain boundary (gb) and electrode (elec) contributions. (E) Measured data and fit result using the circuit shown in (D). (F) Total and bulk conductivity extracted from the impedance spectroscopy data.

Fig. S2 (A-C) shows the temperature dependent impedance spectroscopy data of LSnPS. At low temperatures, suppressed semicircles containing both bulk and grain boundary contributions are observed. At higher temperatures, see Fig. S2 (C), due to the low impedance of the sample, inductive effects arising from the wiring are increasingly observed at high frequencies. The total impedance can be read out easily at all temperatures, see full triangles in Fig. S2 (F). The bulk contribution can be extracted from the data using the equivalent circuit shown in Fig. S2 (D). Independent of the temperature, the bulk capacity obtained from the fit was in the 10 pF range, the grain boundary (gb) capacity was in the nF range, and the electrode capacity was in the μF range. As expected from the setup, the stray capacity was in the pF range. The bulk conductivities obtained from the fit are included into Fig. S2 (F) as open triangles and follow Arrhenius behavior activated with 0.25 eV with the RT conductivity being 4 mS/cm.

S6: Estimation of the maximum electronic transference number

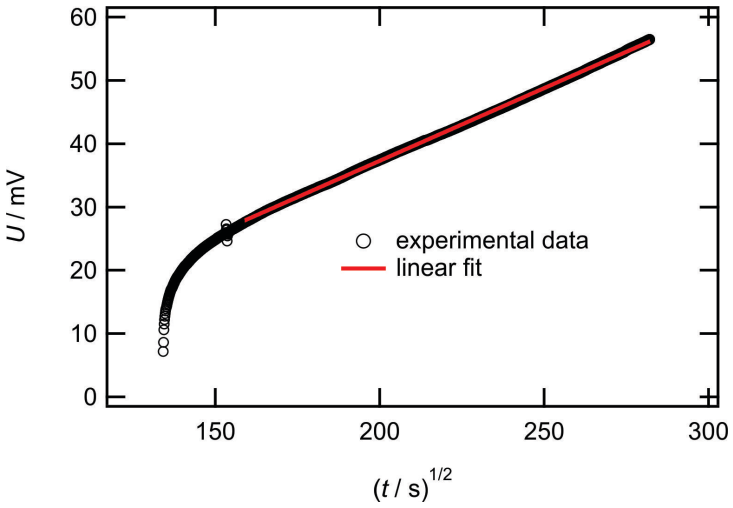

Figure S3: Polarization curve of an Au|LSnPS|Au cell for an applied current of 1 nA at 200°C. The measured voltage is displayed vs. the square root of the time.

As the steady state could not be waited for, we cannot determine the electronic conductivity values but we can reliably give an upper limit. We achieve this in two independent ways:

(i) From Figs. 5b or S3 we deduce directly $U(\text{steady state}) > 60$ mV and hence $\sigma_{\text{eon}} < 2 \cdot 10^{-7}$ S/cm, thus $t_{\text{eon}} < 3 \cdot 10^{-6}$.

(ii) The $\sqrt{t}$ plot of the polarization voltage (Fig. S3) shows a linear behavior as expected for chemical diffusion for times $< \tau_\delta$, for which the transient is described by the following relation (see, *e.g.* Ref. [9]):

$$U = \frac{iL}{\sigma} + \frac{\sigma_{\text{ion}}}{\sigma} \cdot \frac{iL}{\sigma_{\text{eon}}} \cdot \frac{4}{\pi^{\frac{3}{2}}} \sqrt{\frac{t}{\tau_\delta}}$$

The comparison of the polarization curve shown in Fig. S3 with the above equation shows an additional fast polarization process for small times, probably phase boundary polarization; yet the square-root time dependence describing semi-infinite chemical diffusion is clearly obvious. As the finite (exponential) diffusion part is not yet seen, this provides a lower limit for τ_δ and the corresponding chemical diffusivity of $\widetilde{D}_{\text{Li}} < 10^{-14}$ m^2/s at 200 °C. The upper limit of the electronic conductivity is obtained from the slope of U *vs.* $\sqrt{t}$ with $\frac{\sigma_{\text{ion}}}{\sigma} \approx 1$ and the lower limit of τ_δ. The upper limit of the electronic conductivity amounts to $\sigma_{\text{eon}} < 10^{-7}$ S/cm at 200 °C corresponding to an electronic transference number of $t_{\text{eon}} < 1.4 \cdot 10^{-6}$.

S7: SEM-EDX results on $Li_{11}Si_2PS_{12}$

Spectrum	Si	P	S
Spectrum 1	11.86	5.60	82.53
Spectrum 2	12.77	6.67	80.56
Spectrum 3	14.80	5.86	79.34
Spectrum 4	12.61	7.14	80.25
Spectrum 5	12.44	6.05	81.51
Spectrum 6	13.13	6.36	80.51
Mean	12.94	6.28	80.78
Std. dev.	1.00	0.56	1.10

All results in atomic%

The theoretical values for $Li_{11}Si_2PS_{12}$ are 13.33 % Si, 6.66 % P, 80 % S (Si:P:S = 2:1:12). As expected (and intended) from the synthesis route, a slight excess of S is observed. Nevertheless, within the standard deviation of 1%, the theoretical values are obtained.

S8: Redox stability of $Li_{10}SnP_2S_{12}$ and $Li_{10}GeP_2S_{12}$

Stability against Li metal:

Both $Li_{10}SnP_2S_{12}$ and $Li_{10}GeP_2S_{12}$ heavily react with molten Li under ignition. Therefore, one has to assume that the observed stability of $Li_{10}GeP_2S_{12}$ against Li at room temperature[10] relies on the formation of a passivation layer.

Redox stability:

In order to study the redox stability and the formation of a passivation layer for $Li_{10}SnP_2S_{12}$ and $Li_{10}GeP_2S_{12}$, we constructed cells with the following setup: Li|EC:DEC:$LiPF_6$|$Li_{10}SnP_2S_{12}$|Au (EC: DEC = 1:1, $c(LiPF_6)$ = 1 mol/l, EC…ethylene carbonate, DEC…diethyl carbonate). This setup avoids direct contact of the electrolyte with Li metal and thus allows the study of the processes occurring at higher potentials.

- The open-circuit voltage (OCV) of the cells is 2.4 V in both cases (see Figs. S4A and S4B). This value is typical for sulphides.
- When the potential is increased (starting from the OCV), a large cathodic peak is observed at 2.6 V - 3 V, which can be assigned to sulphide oxidation (not shown).
- When the potential is decreased (starting from the OCV), the first anodic peak observed occurs at 1.4 V for $Li_{10}SnP_2S_{12}$ and more pronounced at 1.3 V for $Li_{10}GeP_2S_{12}$ (see Figs. S4A and S4B). This peak can tentatively be ascribed to thiophosphate reduction.
- The second anodic peak occurs at 0.8 V for $Li_{10}SnP_2S_{12}$ and at 0.6 V for $Li_{10}GeP_2S_{12}$. These peaks probably correspond to thiostannate and thiogermanate reduction, respectively.

The anodic and cathodic peaks limit the *thermodynamic* electrochemical window to the small (but not unexpectedly small) potential range between 1.4 V and 2.6 V. The reported behavior of $Li_{10}GeP_2S_{12}$, which suggested a much larger electrochemical window, therefore, has to be due to the formation of passivation layers (SEI).

Formation of stable passivation layers:

Since Kanno *et al.* found stable cycling in the setup Li|$Li_{10}GeP_2S_{12}$|Au (see Ref. [10]), we have to assume that $Li_{10}GeP_2S_{12}$ readily forms a stable passivation layer in contact with Li metal at room temperature. In our measurements we found that a steady state is obtained after 7 cycles between 2.5 V and −0.5 V (1 mV/s) using the setup described above. After this treatment, the material is stable against higher potentials as well, and stable cycling was observed in the voltage range between −0.5 V and 4 V for at least 10 cycles (see Fig. S4D).

In the case of $Li_{10}SnP_2S_{12}$, the passivation layer has to be formed at slightly higher potentials, *i.e.* it does not form in contact with metallic Li. Therefore, we cycled the cell several times from 2.5 V to 1.0 V, then to 0.8 V, 0.6 V, 0.4 V, 0.2 V and 0 V, respectively. After this treatment, a stable SEI is formed which then allows the cycling in the voltage range between −0.5 V and 4 V for at least 10 cycles (see Fig. S4C), which is the same as observed for $Li_{10}GeP_2S_{12}$. In a potential all-solid-state battery, *e.g.* Sn, Si, In, or lithium titanate anodes could be used. Hereby, a suitable program for the first charge cycles has to be employed in order to obtain stable interfaces.

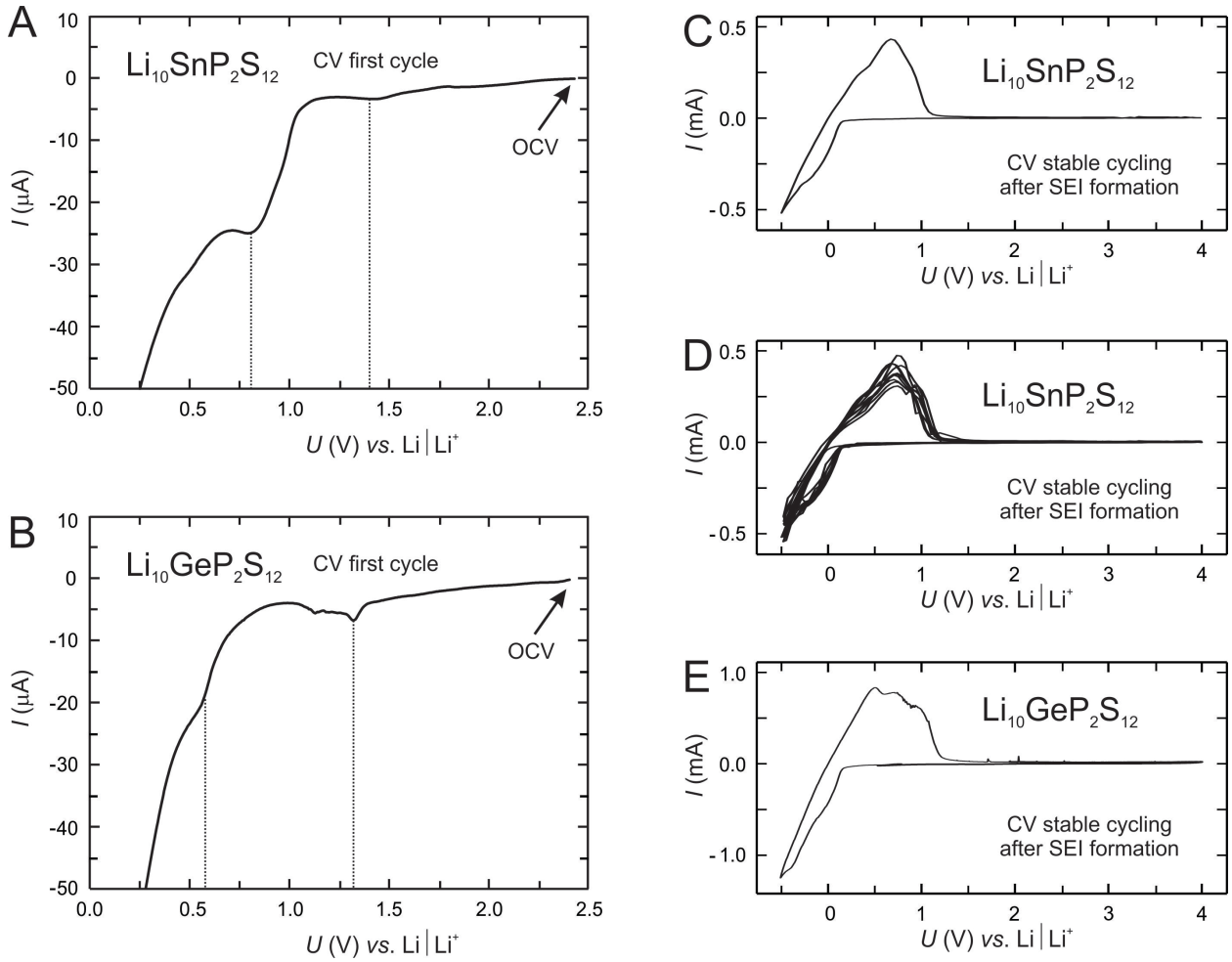

Figure S4: Measurements on cells of the setup Li|liquid electrolyte|solid electrolyte|Au. **A and B:** first cycle from the OCV to lower potentials for $Li_{10}SnP_2S_{12}$ and $Li_{10}GeP_2S_{12}$, respectively. **C and D:** stable cycling behavior (C: one cycle, D: 10 cycles) between −0.5 V and 4 V for $Li_{10}SnP_2S_{12}$ after the formation of stable passivation layers. **E:** stable cycling behavior between −0.5 V and 4 V for $Li_{10}GeP_2S_{12}$ after the formation of stable passivation layers.

[1] T. Kaib, S. Haddadpour, M. Kapitein, P. Bron, C. Schröder, H. Eckert, B. Roling, S. Dehnen, *Chem. Mater.* **2012**, *24*, 2211.

[2] M. Murayama, R. Kanno, M. Irie, S. Ito, T. Hata, N. Sonoyama, Y. Kawamoto, *J. Solid State Chem.* **2002**, *168*, 140.

[3] E. O. Stejskal, E. O. Stejskal, J. E. Tanner, *J. Chem. Phys.* **1965**, *42*, 288.

[4] A.Kuhn, V. Duppel and B. V. Lotsch *Energy Environ. Sci.* **2013**, *6*, 3548.

[5] A. Kuhn, J. Köhler, B. V. Lotsch, *Phys. Chem. Chem. Phys.*, **2013**, *15*, 11620.

[6] *P.* Bron, S. Johansson, K. Zick, J. Schmedt a. d. Günne, S. Dehnen, B. Roling*, J. Am. Chem. Soc.* **2013**, *135*, 15694.

[7] N. Bloembergen, E. M. Purcell, R. V. Pound, *Phys. Rev.* **1948**, *73*, 679.

[8] J. S. Waugh, I. Fedin, *Sov. Phys. – Solid State,* **1963**, *4*, 1633.

[9] J. Maier, in: C. Vayenas, R. E. White, M. E. Gamboa-Aldeco (eds.), *Modern Aspects of Electrochemistry*, Springer, **2007**, *41*, 95.

[10] N. Kayama, K. Homma, Y. Yamakawa, R. Kanno, M. Yonemura, T. Kamiyama, Y. Kato, S. Hama, K. Kawamoto, A. Mitsui, *Nat. Mater.* **2011**, *10*, 682.